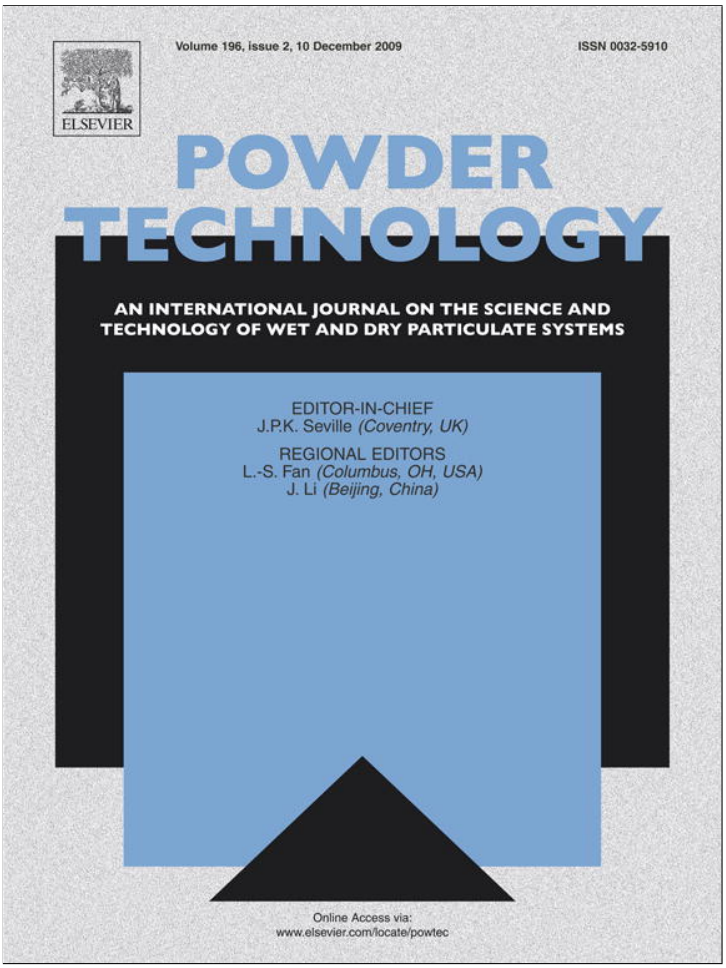

Powder Technology 196 (2009) 202–212

Contents lists available at ScienceDirect

Powder Technology

journal homepage: www.elsevier.com/locate/powtec

# Machine vision based particle size and size distribution determination of airborne dust particles of wood and bark pellets

C. Igathinathane [a,b,*], S. Melin [b,c], S. Sokhansanj [b], X. Bi [b], C.J. Lim [b], L.O. Pordesimo [d], E.P. Columbus [a]

[a] Department of Agricultural and Biological Engineering, Mississippi State University, 130 Creelman Street, Mississippi State, MS 39762, USA
[b] Department of Chemical and Biological Engineering, University of British Columbia, 2360 East Mall, Vancouver, BC, Canada V6T 1Z3
[c] Delta Research Corporation, 501 Centennial Parkway, Delta, BC, Canada V4L 2L5
[d] ADM Alliance Nutrition, 1000 North 30th Street, Quincy, IL 62301, USA

ARTICLE INFO

*Article history:*
Received 10 April 2009
Received in revised form 6 July 2009
Accepted 31 July 2009
Available online 11 August 2009

*Keywords:*
Dust
Wood pellet
ImageJ plugin
Particle size distribution
Physical property
Image processing

ABSTRACT

Dust management strategies in industrial environment, especially of airborne dust, require quantification and measurement of size and size distribution of the particles. Advanced specialized instruments that measure airborne particle size and size distribution apply indirect methods that involve light scattering, acoustic spectroscopy, and laser diffraction. In this research, we propose a simple and direct method of airborne dust particle dimensional measurement and size distribution analysis using machine vision. The method involves development of a user-coded ImageJ plugin that measures particle length and width and analyzes size distribution of particles based on particle length from high resolution scan images. Test materials were airborne dust from soft pine wood sawdust pellets and ground pine tree bark pellets. Subsamples prepared by dividing the original dust using 230 mesh (63 μm) sieve were analyzed as well. A flatbed document scanner acquired the digital images of the dust particles. Proper sampling, layout of dust particles in singulated arrangement, good contrast smooth background, high resolution images, and accurate algorithm are essential for reliable analysis. A "halo effect" around grey-scale images ensured correct threshold limits. The measurement algorithm used Feret's diameter for particle length and "pixel-march" technique for particle width. Particle size distribution was analyzed in a sieveless manner after grouping particles according to their distinct lengths, and several significant dimensions and parameters of particle size distribution were evaluated. Results of the measurement and analysis were presented in textual and graphical formats. The developed plugin was evaluated to have a dimension measurement accuracy in excess of 98.9% and a computer speed of analysis of <8 s/image. Arithmetic mean length of original wood and bark pellets airborne dust particles were $0.1138 \pm 0.0123$ and $0.1181 \pm 0.0149$ mm, respectively. The airborne dust particles of wood and bark pellets can be described as non-uniform, finer particles dominated, very finely skewed with positive skewness, leptokurtic, and very well sorted category. Experimental mechanical sieving and machine vision methods produced comparable particle size distribution. The limitations and merits of using the machine vision technique for the measurement of size and size distribution of fine particles such as airborne dust were discussed.

Published by Elsevier B.V.

## 1. Introduction

Dust in industrial environment is an undesirable byproduct considered as a pollutant, hence needs proper management. Based on the type of industrial source dust can be classified as organic and inorganic dust. Dust particles occur over a range of particles sizes. From occupational health view point, dust are categorized as respirable (<10 μm), inhalable (median diameter 10 μm), and total dust covering both [1]. When the dust particle sizes are small and depending on the particle density, they become airborne and pose more serious issues than larger particles that easily settle out. Industrial dust issues include health hazards (e.g., respiratory, irritation to organs and skin), dust explosions and fire, equipment damage, impaired visibility, unpleasant odors, and problems in community relations [1], apart from being an inconvenience to plant operators. Determination of size and size distribution of the dust particles is fundamental to characterization of dust that is vital for designing handling devices and developing management strategies (prevention, control, dilution or isolation).

The wood pellets industry in Canada with total sales of $\$2 \times 10^5$ mainly as biofuel in European Union nations is an important component of Canada's rural economy [2], but dust is a serious concern if not yet a problem. Organic dust in pelleting industries like that in grain industries, presents the outlined dust related issues

* Corresponding author. Tel.: +1 662 325 3365; fax: +1 662 325 3385.
*E-mail addresses:* igathi@gmail.com, ic43@msstate.edu (C. Igathinathane).

0032-5910/$ – see front matter. Published by Elsevier B.V.
doi:10.1016/j.powtec.2009.07.024

during pellets production, handling, storage, and transport. Dust is produced during handling the particulate wood before pelleting (grinding, and handling), and after pelleting (breakage during cooling, handing, storage, and shipment). Self-heating and explosivity of dust in pellet industries may lead to catastrophic damages, as the pellets are energy densified fuels unlike agricultural grains, hence warrant strict and careful management.

Assessment of particle size and size distribution of dust, an essential first stage measurement, can be obtained utilizing several methods such as the basic mechanical sieving, and advanced light scattering, acoustic spectroscopy, and laser diffraction methods. Sieve analysis based approach, although considered as a standard method, cannot be considered as an accurate method of classifying the particulate materials by length [3–5]. Direct measurement of a large number of particles using travelling microscopes would be tedious. However, advanced instruments providing quicker results are highly expensive and sophisticated. Some of the indirect advanced methods involving scattered or diffracted light or laser assume the particle to be spherical, which is not always the predominant case with natural particulate materials.

Machine vision is another approach to measure the size of particulate material, and image processing techniques were actually used for calibrating the aforementioned advanced instruments. Reviews on various machine vision research in such areas as robotic weed control, food quality evaluation, grading, inspection, classification, analysis of several agricultural and food products, and the merits and limitations of machine vision systems, as well as fish eggs counting from scanned images are available [6–9]. The machine vision applications using high-end proprietary software reported in literature generally tend to be expensive. A simpler and elegant alternative to this approach is user-coded plugin programs developed using ImageJ. ImageJ developed at the National Institutes of Health (NIH), USA is a Java-based public domain image processing and analysis program, which is freely available, open source, multithreaded, and platform independent [10] that can be utilized to develop user-coded plugins to suit the specific requirements of any conceived application. ImageJ offers tools for the development of user-coded macros and plugins that can be tailored to suit specific image processing applications [11,12]. Analyzing digital images with a user-coded ImageJ plugin has been shown to be an alternative method with good accuracy for the determination of size and size distribution of particulate materials [13,14].

This research to determine the size and size distribution of airborne dust from the wood pellet industry, in most part, follows the method outlined in our previous efforts [4,5,13,14]. Since airborne dust particles are minute, accurate measurement requires high resolution images that can effectively "capture" the physical dimensions of dispersed dust particles. It can be shown that the input image quality in terms of its resolution directly affects the accuracy of the measurements. For cost containment and wider applicability, it was a conscious choice in this research that a flatbed document scanner available in retail be used as the image acquisition device. The particle size distribution will be analyzed based on length, the most significant dimension, in a sieveless manner using distinct dimensioned particles [5]. A host of several parameters describing the size distribution of dust particles will be also evaluated. The objectives of this research were to apply our sieveless particle size distribution analysis plugin [5] after suitable development to handle fine airborne dust particles, evaluate the plugin size measurement accuracy, and compare the particle size distribution with mechanical sieving.

## 2. Experimental

### 2.1. Airborne dust samples and sampling procedure

The airborne dust samples from pelleting operations were collected from the baghouse deposits. Airborne dust samples from pelleting sawdust of soft pine (*Pinus* spp.) wood (Fibreco, Vancouver, British Columbia, Canada) and from pelleting ground bark of pine tree trunk (Enligna, Nova Scotia, Canada) were used as test materials. It is often followed in dust or fine particulates analysis to divide the dust by a 230 mesh sieve (63 μm) and analyze them separately. Therefore, subsamples were prepared for wood and bark pellet dust by subjecting the original dust through the 230 mesh sieve as overflow and underflow. The original (unseparated) and overflow and underflow subsamples (separated by 230 mesh) of the two materials were held in individual Ziploc® bags (total six samples). The test materials were stored in air-conditioned laboratory environment (about 22 °C and 55% RH) before the experiments.

For sampling, the dust in each bag was thoroughly mixed by shaking the contents and turning with a spatula, and a scoop (~2–3 g) was obtained with a spoon. The dust was poured into a heap on a clear sheet of paper. Then the heap was spread using a strong-thin cardboard by gentle vertical chopping motion, first along one direction and then in the direction perpendicular to that. Cardboard was used as it did not cause electrostatic attraction of the dust particles. This chopping action causes the dust heap to spread uniformly into a thin bed of dust. Using the cardboard, small squared areas of spread dust were separated as the selected samples for the experiment. Care was taken to recover all the particles from the marked areas thereby ensuring that a true representation of the spectrum of the particle sizes in the dust is maintained. Thus, proper mixing of the bulk dust and meticulous spreading and dividing ensure that the drawn samples to represent the original bulk. Final mass of sample used for image acquisition was about 100 to 200 mg.

### 2.2. Dust sample layout for imaging

A flatbed document scanner (4800×9600 DPI; Cano-scan 4400F, Canon USA. Inc., Lake Success, NY, USA) was used to acquire the color images of dust particles. The aim was to spread the individual dust particles so that they did not touch or overlap with the other particles (singulated arrangement) for better image quality and easier analysis. Singulated arrangement of particles, followed in the study, simplifies the analysis and eliminates the need for advance image handling methods such as erosion–scrap–dilation procedures to resolve non-singulated particles [15]. However, in a fish eggs counting study the Optimas image processing system (Ver. 6.5) applied an erosion–dilation filter to separate touching eggs from a single cluster to the component individual eggs [9]. In this study, to make the image analysis simple, the problem of particles touching was addressed by manual separation of particles, as explained subsequently, at the source itself rather than at the later image preprocessing stage.

A good quality overhead projector transparent sheet covered the scanner bed. This forms an intermediate layer protecting the scanner glass bed and aids in removing the sample quickly. A 3/4″ flat art brush with smooth bristles was utilized to pick up the divided batches of dust and transfer the dust to the scanner bed. The brush with dust particles were held over the scanner bed by about 150 mm and bristles were stroked using the thin cardboard. This caused the dust particles to fly down and settle on the scanner bed. Stroking was repeated to dislodge all the dust particles from the brush till it was clean. The process of picking the dust and depositing them by stroking was repeated until the sample was spread completely. During each deposition, the brush was moved to across and down the scanner bed area. Sprinkling of the picked up dust uniformly on the scanner to achieve singulated arrangement of dust particles is the critical step. Since sporadic touching and overlapping of particles cannot be avoided, those particles were identified using an illuminated magnifier and moved around using a pointed knife (X-ACTO, #11, Elmer's Products, Columbus, Ohio, USA). Although the entire procedure takes some time (10 min or less based on the dust particle characteristics for an area of 216×279 mm (8.5″×11″) that produces about 10 image samples), singulated arrangement of dust particles was practically achievable. One pixel gap between particles is

as good as a huge gap between particles in constituting a singular arrangement for the analysis. To achieve good contrast a black background (oil painted special quality art paper) was carefully placed over the sprinkled dust. If the background paper quality was not good, then the fiber matrix of the paper will be captured and that impairs the quality of the acquired digital image.

### 2.3. Image acquisition

The maximum image size that the scanner can capture was 21,000×30,000 pixel in the horizontal and vertical directions respectively; hence an image can have a maximum of $6.3\times10^8$ pixels. Actual physical dimensions of the objects scanned were decided based on the resolution setting in terms of dots per inch (DPI) values, which can be set through advanced settings in the scanner software. For instance, at 6350 DPI an image having 20,826×29,982 pixel represents a physical dimension of about 83×120 mm, with each square pixel having a physical dimension of 4 μm, and the resulting image file size was 17.14 MB. Therefore, DPI settings directly influence the accuracy or resolution of the image and indirectly influence the physical size of the image acquired. In this research, we used a 6350 DPI with physical dimension of 50.8×50.8 mm (12,700×12,700 pixel) for the images that had a mean file size of 5.9 MB. Although digital pictures from the digital camera are equally applicable for image analysis, the DPI will be usually low (e.g., <200 DPI for a 5 megapixels camera). Therefore, unless specialized digital cameras with high zoom capacity were used, common digital cameras cannot be used to analyze airborne dust particles.

After proper layout of dust on the scanner bed (216×297 mm) the images can be scanned by fixing the 50.8 mm square image window at desired location on the whole view. Successive images can be easily captured by moving image window and performing the scans. Ten images were acquired from single layout of the dust and these served as replications. The procedure was repeated for all samples of different material (wood and bark dust), sieve separation (original, overflow and underflow of 230 mesh), and replications (10). Thus 60 images were obtained and analyzed.

### 2.4. Image preprocessing

Image processing algorithms require a binary image that can be produced by converting the colored image first into grey-scale image and then into binary image by proper thresholding. The procedure of obtaining the binary image using ImageJ commands is similar to that reported earlier [5,13,14]. ImageJ's "*Threshold…*" command by default produces the auto-threshold limits, wherein the lower limit is varied with the image and higher limit was at the maximum of 255. Since the dimensions of dust particles are very small, thresholding operation is critical; and auto-threshold serves better as it is an optimized method. Properly identified particles by auto-thresholding display a "halo effect" showing pixels of lighter color around the particles (Fig. 1).

Very high particle density in the image may cause the auto-threshold to fail, and the occurrence of this failure during normal particle layout is very limited. This auto-threshold failures can be addressed either by discarding the image for fresh layout of particles with reduced density or using the image with manual thresholding at preprocessing. In manual thresholding, the lower threshold limit was adjusted so that each particle was surrounded by about a single pixel band of lighter grey around the object boundary displaying the "halo effect." Reducing the lower threshold limit further will make the object grow in size and consuming the boundary halo. We verified that for accurate dimensional measurements using objects of known dimensions that this "halo effect" is essential; and the default auto-threshold usually produces this correctly. Proceeding with the correct threshold limits creates the required binary image. Options such as "*Exclude on Edges*" and "*Include Holes*" while running the ImageJ's "*Analyze Particles*" routine were selected. These options ensure including all whole particles and ignoring

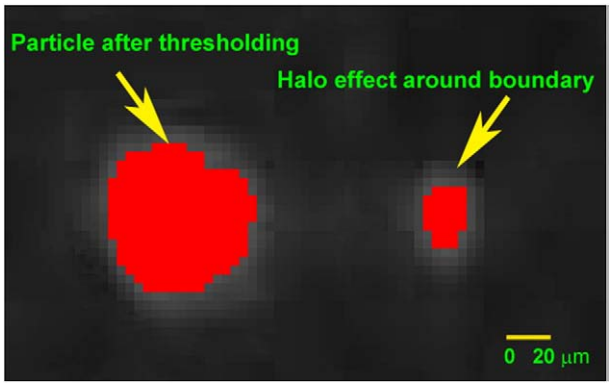


**Fig. 1.** "Halo effect" around dust particles during thresholding for grey-scale images.

holes, if any after thresholding, in the particles of the image during analysis. If the object is properly covered by thresholding, then accurate size measurement is automatically guaranteed as the image processing method is direct in principle. Measurement accuracy improves with increase in DPI. Capacity of the input device (DPI and total number of pixels captured), and the 32-bit operation of ImageJ with common computing device restricts the handling and accuracy. A 64-bit ImageJ operation requires advanced specialized computers. When high resolution images with increased DPI are sought, restriction also comes in the form of reduced physical dimensions of the image window that reduces the number of particles included in the analysis. High resolution obviously increases the handled file size of the image.

### 2.5. Image calibration

Image calibration is required to correlate the image dimensions in pixel to physical dimensions. Calibration is also needed to account for images acquired with different resolutions (DPI). From the calibration procedure a scale factor (mm/pixel) can be determined. The scale factor can be calculated directly as 25.4/DPI (mm/pixel) from the image DPI information. The DPI or resolution information of any image is retrieved from the image properties from several applications (e.g., MS Windows Explorer, scanner software). The DPI value of the original color image should be used for calibration. Our developed ImageJ plugin takes the DPI value as input and calculates the scale factor. The plugin was coded so that it needs calibration only once at the start of a multiple measurement session or as required. Whatever calculated scale factor in the initial session was stored in a text file and retrieved for subsequent measurements from the stored file.

### 2.6. Dimensions determination methodology in plugin

Dust particle shapes are irregular, and assuming them to be of regular geometrical shapes will result in oversimplified approximation. Particle's maximum dimension, obtained from the outline, was considered as the length in this work. The built-in standard measurements such as Feret's diameter of ImageJ's "*Analyze Particles…*" can be advantageously used for length measurements. The Feret's diameter also known as caliper length represents the diameter of the circumscribed circle or the longest distance between any two points along the object boundary. This method of length determination is uniformly followed to all particles of the sample. Widths of dust particles were determined following the "pixel-march" method [5], which is similar to the reported pixel-march method used with food grains [14].

The pixel-march method works effectively for convex shapes. As most of the particulate material such as ground biomass are predominantly convex shaped (≤4.4% nonconvex), we utilized the same pixel-march strategy of the [5], but accounted for those nonconvex shapes using a different approach as described subsequently. In addition, we

incorporated a few more size distribution parameters and sieving simulation for mechanical sieving comparison into the plugin. It is expected, as well as subsequently shown in results, that the airborne dust particles' shape will be mostly convex as they are minute when compared to the larger particles of hammer-milled biomass. However, for nonconvex shapes that identified by the location of centroid outside the particle boundary the widths were determined from the minimum of minor axis and bounding rectangle dimensions (Fig. 2). Handling of nonconvex shapes in this manner will not be as accurate as the pixel-march width of convex shape but will result in slight overestimation. Thus a plugin that evaluates convex shaped particles should work well with airborne dust particles with the mentioned modifications. A good alternative option for width is to use the minimum Feret's diameter, recently made available as ImageJ built-in standard measurement, which however results in width overestimation for nonconvex curved particles.

For widths of very small particles represented by areas <12 pixels (e.g., 4×3 or 3×4 pixel matrix), the minor axis of the particles were directly used rather than to resort to pixel-march. "*Fit ellipse*" and "*Feret's diameter*" measurement options should be chosen to ensure obtaining these standard ImageJ results. The procedure using Feret's diameter and pixel-march for length and width respectively makes accurate and back traceable measurements. When a particle encroaches another curved nonconvex particle's bounding rectangle and when the centroid of the first particle falls inside the boundary of the second, the nonconvex particle will be misidentified as convex and the pixel-march method reports inaccurate width measurement. This scanty possibility constitutes one of the limitations of the plugin. Complete description of the plugin development can be found elsewhere [5].

It should be noted the Feret's diameter determined lengths of all particles irrespective of particle size, shape, and orientation as a consistent method; however, the method of width determination varied based on particle size and shape as discussed already. It is also possible to identify and filter out some of the particles from the analysis based on particle size and/or shape to render uniform width determination method. Nevertheless, in the interest of better representation of the sample we included all particles in the analysis despite the differential treatment on width determination.

### 2.7. Sieveless particle size distribution analysis

Length being the dominant dimension compared to width as well as length has significance in sieving process, it was considered as the working dimension for the size distribution analysis in the present study. Sieveless particle size distribution analysis based on distinct particles was followed in this work wherein particle lengths determined by machine vision were grouped into categories of particles of distinct lengths and analyzed for size distribution [5]. The sum of groups of particles represented by distinct length particles actually makes up the total number of particles of the sample. This distinct lengths grouping of particles, obtained without sieves by machine vision, can be thought of the separation and grouping distinct particles mechanically by a set of numerous ideal theoretical sieves. The true measurement and separation of particles into groups based on any selected parameter (e.g., length, width, area) can be easily achieved by image processing methods but not by standard mechanical sieving.

### 2.8. Particle size distribution parameters

Representative cumulative dimensions such as $D_{95}$, $D_{90}$, $D_{84}$, $D_{75}$, $D_{60}$, $D_{50}$, $D_{30}$, $D_{25}$, $D_{16}$, $D_{10}$, and $D_5$ describing the particle size and their distribution were derived from the cumulative undersize characteristics of original particle dimensions data. Linear interpolation of the cumulative undersize of distinct length groups gave these representative dimensions. Several common descriptive parameters of the particle size distribution evaluated in this study are defined and presented in Appendix A. Some parameters such as minimum, maximum, arithmetic mean, skewness, and kurtosis were evaluated both for length and width.

### 2.9. Calculation methodology in plugin

A brief outline of overall calculation methodology in the plugin is shown in Fig. 3, which is similar to the procedure reported earlier [5,14]. Individual particles from the binary image were identified from left to right and top to bottom. For these identified particles various standard properties were retrieved and required dimensions and parameters were calculated and stored. Outputs of the analysis from the developed plugin include plots of length of all particles, frequency distribution, and cumulative distribution of particles along with results in text file format.

To estimate the accuracy of the machine vision method, 10 Basmati rice grains were randomly selected and the maximum dimensions measured using digital calipers (0.01 mm accuracy) were compared with the particle lengths from the image.

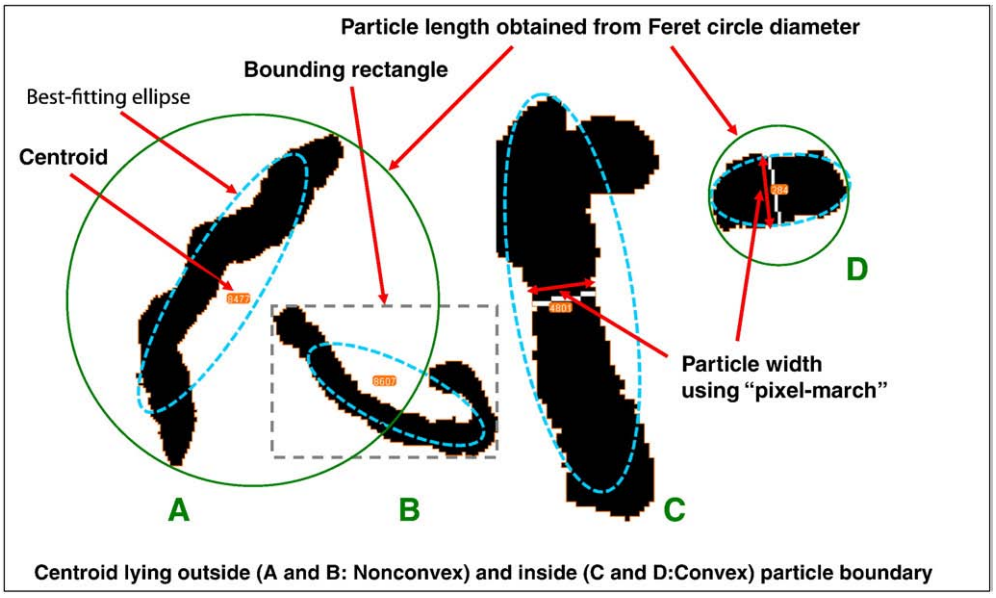


**Fig. 2.** Particle dimension measurement using Feret's diameter and pixel-march methods.

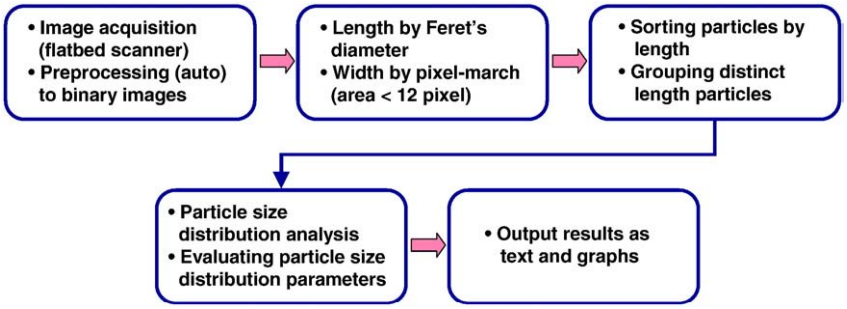


**Fig. 3.** Process flow in the developed machine vision plugin.

### *2.10. Mechanical sieving and plugin provision for comparison*

Experimental particle size distribution was obtained using mechanical sieve shaker and standard sieves for original airborne dust of wood and bark pellets. A private commercial laboratory performed the mechanical sieving tests. The sieve set consisted of 40 (0.425), 70 (0.212), 100 (0.150), 200 (0.075), and 230 mesh (0.063 mm) sieves and a pan. Pittsburgh steam coal and Lycopodium spores were used as reference materials. Moisture contents of these materials were determined as 5.6%, 7.9%, 0.0%, and 4.0% wet basis for wood pellet dust, bark pellet dust, Pittsburgh steam coal, and Lycopodium spores, respectively. Materials retained in each sieve after completion were expressed in percentages. Sieve simulation with same sieve openings to match this mechanical analysis was provided in the plugin. Additional codes were included in the plugin that grouped the sorted distinct dimensioned particles based on these specific sieve opening dimensions (six groups) and expressed in percentages for direct comparison. Five arbitrarily selected images of original wood and bark pellets dust were used and the means with standard deviation were reported for machine vision analysis comparison.

## 3. Results and discussion

### *3.1. Graphical outputs of airborne dust particle size measurement and analysis*

Although the original image acquired was in color (Fig. 4A), the plugin actually operates on the preprocessed binary image (Fig. 4B) based on the described algorithm and produces textual and graphical outputs (Fig. 4C–E). The number of particles in the image, of a physical dimensions of $50.8 \times 50.8$ mm, was in excess of 5000. Images also depict that using the outlined dust particle layout procedure (Section 2.2), it is fairly easy to achieve the singulated arrangement of particles; however, occasional deviations cannot be avoided but will have minimal effect on the analysis. The number of curved particle with centroid falling outside object boundary was found to be highly limited. For instance, the number of such nonconvex particles in this case was $0.74 \pm 0.14\%$ for wood and $0.94 \pm 0.22\%$ for bark pellet airborne dust particles.

The graphical outputs such as individual plot of particle lengths, frequency plot of selected quantiles (20) of the entire particle length range, and cumulative under size of distinct length particles give comprehensive information about the particle size distribution (Fig. 4C, D, and E). The plot of individual particle length allows for easy overall visualization and approximate comparison of particle lengths among samples, especially for longer particles. In the example plot (Fig. 4C), the number of particles $>1.0$ mm or $>0.5$ mm were smaller for wood pellet airborne dust than bark pellet airborne dust. However, the frequency and cumulative undersize distributions (Fig. 4C and D) show that the finer particles completely dominated the distribution and the particles longer than 0.5 mm were less significant. Graphical outputs are excellent standard tools to represent and compare particle size distribution of different samples. Similar graphical trends were observed with other sample images.

### *3.2. Dimension based particle size distribution outputs of airborne dust particles*

Mean values of 10 images and associated standard deviation of dimension-based particle size distribution descriptors (Table 1) were obtained from the textual results output. The results were categorized as wood and bark pellets as well as grouped under original (unseparated sample), over 63 μm (subsample dust particles retained over 230 mesh sieve), and under 63 μm (subsample dust particles passed through 230 mesh sieve). Results of various evaluated parameters can be interpreted in combination with the definitions listed in Appendix A. Since the accuracy corresponding to 6350 DPI is 0.004 mm (4 μm), the results were reported with four significant digits. The maximum and minimum lengths and widths correspond to specific single particle, while other results correspond to the entire collection of particles. The minimum length and width measured correspond to a particle represented by a single pixel (4 μm square). Therefore, the length and width values of $0.0057 \pm 0.0$ and $0.0039 \pm 0.0$ mm, respectively, were constants values among all groups.

The maximum length of wood and bark pellet airborne dust particles were about 1.6 and 2.1 mm, respectively, with maximum width of about 0.5 mm for both. Arithmetic and geometric mean lengths of wood pellet airborne dust particles on a overall basis were $0.1138 \pm 0.0123$ and $0.0736 \pm 0.0076$ mm, while that of bark dust were $0.1181 \pm 0.0149$ and $0.0607 \pm 0.0071$ mm, respectively. Length/width ratio of overall wood and bark pellet particles was in the range of 2.5 to 3.8 based on both maximum and average dimensions. Thus these ratios indicate that the dust particles are elongated. The arithmetic average length was 1.5 and 1.9 times the geometric average length of the particles for wood and bark pellets, respectively. The reason being the geometric average shifts towards the particle sizes of large proportion i.e. finer particles hence the value is smaller than the arithmetic average. Overall, the arithmetic average lengths fall in the range of $D_{75}$ and $D_{60}$, while geometric average lengths is close to $D_{50}$ and the median value. This observation supports the claim that the geometric average better represents the particle mean length of collection of particles, especially when they deviate from normal distribution. The greater values of geometric average standard deviation (STD) compared with the average values illustrate the wider variation in the length of sample particles.

In general, the divided subsample lots showed the obvious trend of greater and smaller values respectively for over and under 63 μm groups across any cumulative $D$ values (Table 1). However, a clear division of samples around 63 μm was not observed. In other words, particles of smaller dimensions were found in samples that should

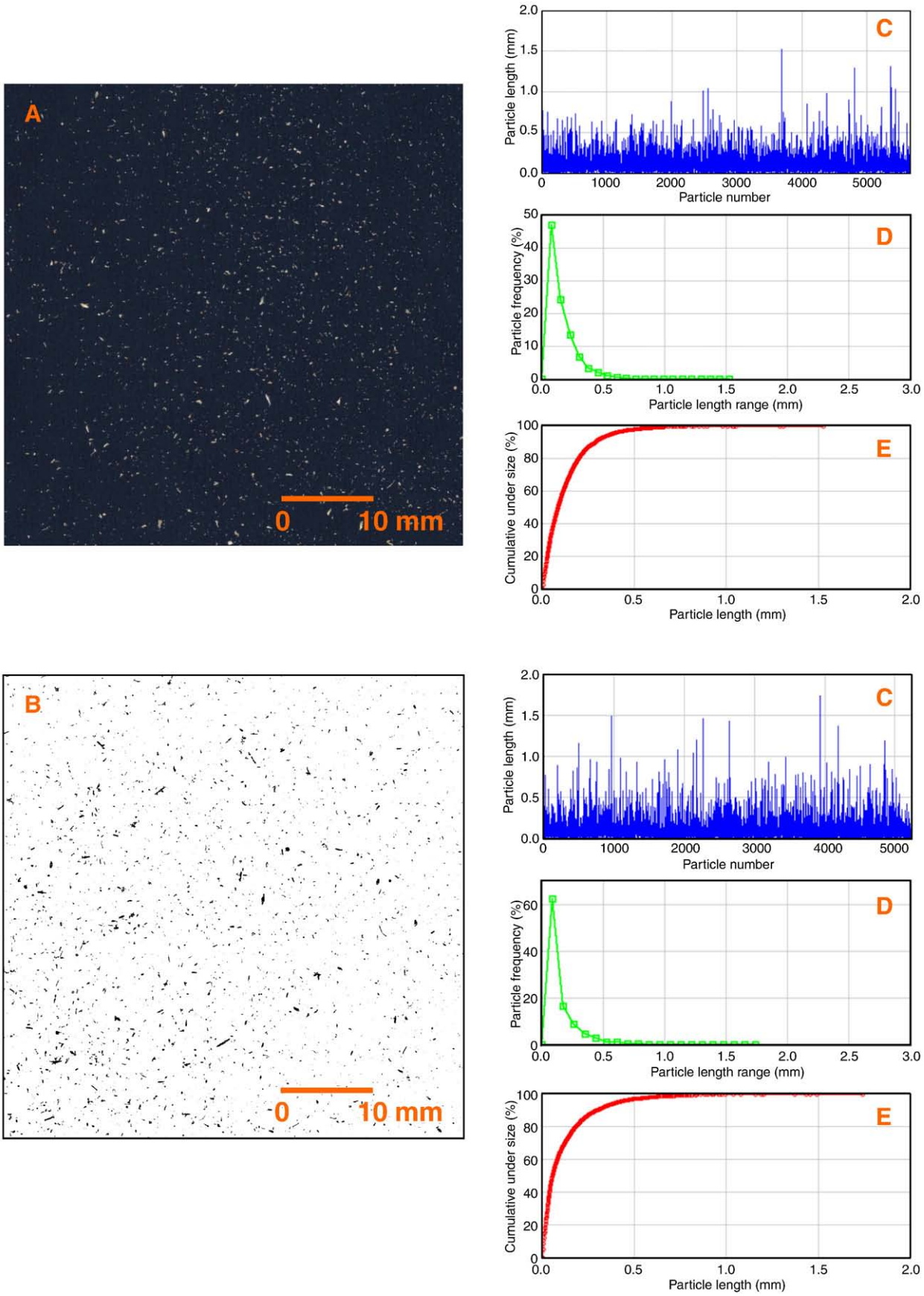


**Fig. 4.** Examples of airborne dust images and analysis graphical results; A – Original color image of wood pellets airborne dust, B – Preprocessed binary image of bark pellets airborne dust, C – Plot of particle lengths of individual particles, D – Plot of percent frequency distribution of particle lengths (20 quantiles), E – Plot of percent cumulative under size of all distinct particle lengths.

**Table 1**
Dimensions based particle size distribution descriptors — all dimensions are in mm.

| Dimension descriptors | Wood pellet airborne dust | | | Bark pellet airborne dust | | |
|---|---|---|---|---|---|---|
| | Original | Over 63 μm | Under 63 μm | Original | Over 63 μm | Under 63 μm |
| Length | | | | | | |
| $D_{95}$ | 0.3234 ± 0.0364 | 0.4162 ± 0.0332 | 0.1982 ± 0.0230 | 0.4226 ± 0.0537 | 0.4763 ± 0.0383 | 0.1723 ± 0.0144 |
| $D_{90}$ | 0.2476 ± 0.0296 | 0.3268 ± 0.0309 | 0.1607 ± 0.0182 | 0.2900 ± 0.0363 | 0.3480 ± 0.0308 | 0.1377 ± 0.0080 |
| $D_{84}$ | 0.1978 ± 0.0233 | 0.2700 ± 0.0280 | 0.1363 ± 0.0149 | 0.2126 ± 0.0309 | 0.2657 ± 0.0289 | 0.1155 ± 0.0057 |
| $D_{80}$ | 0.1749 ± 0.0207 | 0.2429 ± 0.0286 | 0.1256 ± 0.0138 | 0.1774 ± 0.0280 | 0.2258 ± 0.0282 | 0.1047 ± 0.0048 |
| $D_{75}$ | 0.1519 ± 0.0178 | 0.2131 ± 0.0333 | 0.1144 ± 0.0130 | 0.1434 ± 0.0255 | 0.1830 ± 0.0317 | 0.0939 ± 0.0042 |
| $D_{60}$ | 0.1041 ± 0.0122 | 0.1335 ± 0.0543 | 0.0897 ± 0.0114 | 0.0815 ± 0.0147 | 0.0886 ± 0.0307 | 0.0702 ± 0.0037 |
| $D_{50}$ | 0.0814 ± 0.0098 | 0.0926 ± 0.0416 | 0.0764 ± 0.0105 | 0.0591 ± 0.0093 | 0.0497 ± 0.0100 | 0.0584 ± 0.0033 |
| $D_{30}$ | 0.0466 ± 0.0058 | 0.0327 ± 0.0111 | 0.0531 ± 0.0085 | 0.0333 ± 0.0035 | 0.0270 ± 0.0017 | 0.0390 ± 0.0028 |
| $D_{25}$ | 0.0395 ± 0.0048 | 0.0272 ± 0.0058 | 0.0473 ± 0.0074 | 0.0283 ± 0.0028 | 0.0234 ± 0.0011 | 0.0345 ± 0.0034 |
| $D_{16}$ | 0.0280 ± 0.0032 | 0.0191 ± 0.0027 | 0.0360 ± 0.0061 | 0.0193 ± 0.0019 | 0.0167 ± 0.0007 | 0.0255 ± 0.0034 |
| $D_{10}$ | 0.0197 ± 0.0023 | 0.0136 ± 0.0015 | 0.0270 ± 0.0045 | 0.0132 ± 0.0011 | 0.0119 ± 0.0004 | 0.0186 ± 0.0026 |
| $D_5$ | 0.0119 ± 0.0013 | 0.0096 ± 0.0005 | 0.0168 ± 0.0025 | 0.0092 ± 0.0004 | 0.0088 ± 0.0003 | 0.0122 ± 0.0015 |
| Maximum | 1.5875 ± 0.7634 | 1.5776 ± 0.4280 | 1.0495 ± 0.3166 | 2.0854 ± 0.3921 | 2.2439 ± 0.5768 | 1.1165 ± 0.5068 |
| Arithmetic mean | 0.1138 ± 0.0123 | 0.1388 ± 0.0242 | 0.0884 ± 0.0108 | 0.1181 ± 0.0149 | 0.1316 ± 0.0157 | 0.0713 ± 0.0040 |
| Arithmetic mean length STD | 0.1114 ± 0.0134 | 0.1477 ± 0.0100 | 0.0633 ± 0.0073 | 0.1622 ± 0.0192 | 0.1807 ± 0.0159 | 0.0564 ± 0.0066 |
| Geometric mean length | 0.0736 ± 0.0076 | 0.0723 ± 0.0169 | 0.0691 ± 0.0091 | 0.0607 ± 0.0071 | 0.0595 ± 0.0071 | 0.0534 ± 0.0036 |
| Geometric mean length STD | 2.7315 ± 0.1261 | 3.5352 ± 0.1578 | 2.1454 ± 0.0643 | 3.2502 ± 0.1548 | 3.6839 ± 0.1971 | 2.2560 ± 0.1262 |
| Graphic mean | 0.1024 ± 0.0113 | 0.1272 ± 0.0232 | 0.0829 ± 0.0104 | 0.0970 ± 0.0134 | 0.1107 ± 0.0128 | 0.0665 ± 0.0036 |
| Inclusive graphic length STD | 0.0896 ± 0.0110 | 0.1243 ± 0.0113 | 0.0526 ± 0.0056 | 0.1110 ± 0.0154 | 0.1331 ± 0.0124 | 0.0468 ± 0.0035 |
| Width | | | | | | |
| Maximum width | 0.4981 ± 0.1619 | 0.4859 ± 0.0958 | 0.3774 ± 0.0697 | 0.5394 ± 0.1201 | 0.5262 ± 0.0828 | 0.3133 ± 0.0859 |
| Average width | 0.0491 ± 0.0044 | 0.0585 ± 0.0088 | 0.0412 ± 0.0050 | 0.0455 ± 0.0039 | 0.0495 ± 0.0038 | 0.0344 ± 0.0015 |
| Average width STD | 0.0411 ± 0.0051 | 0.0561 ± 0.0036 | 0.0253 ± 0.0025 | 0.0475 ± 0.0042 | 0.0544 ± 0.0032 | 0.0225 ± 0.0028 |

Note: The data reported were: mean ± standard deviation (STD) of 10 image replications. Minimum length = 0.0057 ± 0.0 mm (constant), minimum width = 0.0039 ± 0.0 mm (constant).

have only particles of length >63 μm, and vice versa. The combined effect of ineffective flow of material through the microscopic openings of the sieve and the clumping of fine dust particles due to electrostatic forces may constitute the reason for smaller particles found in the over 63 μm sample. With finer particle such as airborne dust, it is practically impossible to pass all the smaller particles through fine sieves such as 63 μm. "Falling through" effect of lengthier particles [5] and ineffective length separation of sieves [3] were the reasons for observing particles longer than 63 μm in the under 63 μm group. The machine vision approach followed in this research will not have these lacunas, as it divides the particles and groups based on "true length separation" in a sieveless method of analysis on all distinct particles.

### 3.3. Particle size distribution parameters of airborne dust particles

On average, the number of dust particles processed in images ranged from 3220 to 14204 with about 23 ± 13% being distinct particles (Table 2). Observed uniformity index (values 100% representing uniform particles) less than 10.5% indicate that the particles are not uniform. The dust particles had greater variation among lengths as depicted by size range variation coefficients that ranged from 66 to 255%. A wider spread in the lengths was corroborated by larger values of relative span ranging from 1.8 to 6.9. With coefficient of uniformity, any positive deviation from the value of 1.0 indicates non-uniformity among the particles as observed from the values ranging from 3.4 to 9.6. As a comparison, for instance, a fairly uniform natural product such as Basmati rice grains gave a uniformity index of 79.3%, size range variation coefficient of 7.6%, relative span of 0.2, and coefficient of uniformity of 1.1 [5].

Statistical skewness (length>2.0; width>1.5), a measure of data asymmetry, of airborne dust particle lengths and widths were significantly "positively skewed" (critical value = 0.20; $\alpha = 0.01$; $df = 1000$) depicting increased number of smaller particles in the distribution. Statistical kurtosis (length: 8.4–33.6; width: 3.8–15.5), a measure of peakedness of distribution, showed the distribution had significant peak (critical value = 0.28; $\alpha = 0.02$; $df = 2000$). Such distributions with large narrow peak can be described as "leptokurtic." The peak, as seen in Fig. 4D, at the initial was invariably due to the huge collection of tiny particles corresponding to the first of the 20 quantiles. In most cases the smallest particle that can be measured, which is represented by single pixel, makes the largest percentage among other groups.

According to the Folk and Ward (1957) graphical measures classification [16,17], the pellet airborne dust particles were categorized as follows based on the determined graphical parameters shown in Table 2. Both wood and bark pellet airborne dust with inclusive graphic skewness values>0.3 were classified as "very finely skewed." Unlike the statistical moment, based kurtosis having a value of 3.0 for normal distribution, graphic kurtosis value for normal distribution is 1.0. The dust particles mostly belong to "leptokurtic" (1.11–1.50), as noted earlier. And, based on inclusive graphic STD (Table 1), the dust particles fall in the category of "very well sorted" (<0.35). The arithmetic skewness and kurtosis of width distribution followed the length distribution as well.

### 3.4. Particle size distribution of separated dust samples using 230 mesh sieve (63 μm)

A typical plot of cumulative undersize and frequency of original and separated subsamples retained (overflow) over 230 mesh (63 μm) and that passed through (underflow) showed clear separation of distributions (Fig. 5) for both wood and bark pellet dusts. The obvious trend of original sample distribution laid between the separated components distribution was always observed. Overflow being less uniform among the groups (Table 2) had "multimodality" (displaying more than one peak) that can be observed from frequency distribution. Underflow particles had the best uniformity among the groups; therefore the distribution curves displayed smooth variation. Plotting of complete set of processed data will provide the overall trend of all the dust particle groups.

### 3.5. Accuracy of the plugin in dimension measurement

Measurement accuracy is guaranteed upfront while using machine vision procedure, wherein objects were replicated by exact

**Table 2**
Overall particle size distribution parameters and plugin performance.

| Parameters | Wood pellet airborne dust | | | Bark pellet airborne dust | | |
|---|---|---|---|---|---|---|
| | Original | Over 63 μm | Under 63 μm | Original | Over 63 μm | Under 63 μm |
| Total number of particles | 6686 ± 1860 | 3220 ± 695 | 10,581 ± 4886 | 3920 ± 1250 | 3228 ± 445 | 14,204 ± 3644 |
| Total number of distinct particles | 1401 ± 290 | 1192 ± 299 | 1042 ± 297 | 1110 ± 323 | 1099 ± 173 | 979 ± 139 |
| Particles <9 pixels area (%) | 10.09 ± 1.52 | 17.10 ± 2.78 | 6.52 ± 1.56 | 16.82 ± 1.91 | 19.62 ± 1.19 | 10.90 ± 3.05 |
| Nonconvex particles (%) | 0.50 ± 0.64 | 0.87 ± 0.28 | 0.75 ± 0.17 | 1.03 ± 0.22 | 1.02 ± 0.28 | 0.64 ± 0.18 |
| Total CPU time taken (ms) | 6948 ± 879 | 5457 ± 914 | 7870 ± 2439 | 5630 ± 926 | 5276 ± 434 | 8391 ± 1795 |
| Number of particles analyzed/s | 946 ± 182 | 587 ± 67 | 1295 ± 221 | 682 ± 138 | 612 ± 70 | 1683 ± 135 |
| Length | | | | | | |
| Uniformity index (%) | 4.88 ± 0.76 | 2.95 ± 0.28 | 10.47 ± 1.08 | 3.20 ± 0.40 | 2.55 ± 0.29 | 8.87 ± 1.15 |
| Size grade number (mm) | 8.14 ± 0.98 | 9.26 ± 4.16 | 7.64 ± 1.05 | 5.91 ± 0.93 | 4.97 ± 1.00 | 5.84 ± 0.33 |
| Size range variation coefficient (%) | 104.45 ± 8.14 | 168.39 ± 87.08 | 66.13 ± 4.95 | 164.02 ± 13.11 | 255.01 ± 27.59 | 77.25 ± 6.46 |
| Relative span | 2.81 ± 0.24 | 4.23 ± 2.24 | 1.76 ± 0.12 | 4.71 ± 0.37 | 6.93 ± 1.06 | 2.04 ± 0.17 |
| Coefficient of uniformity | 5.33 ± 0.63 | 9.62 ± 3.53 | 3.35 ± 0.21 | 6.16 ± 1.02 | 7.50 ± 2.70 | 3.84 ± 0.56 |
| Coefficient of gradation | 1.06 ± 0.07 | 0.66 ± 0.31 | 1.16 ± 0.04 | 1.04 ± 0.07 | 0.78 ± 0.27 | 1.17 ± 0.08 |
| Statistical skewness | 2.90 ± 1.21 | 2.03 ± 0.30 | 2.68 ± 0.72 | 3.68 ± 0.48 | 3.12 ± 0.50 | 3.05 ± 1.23 |
| Statistical kurtosis | 23.94 ± 39.79 | 8.42 ± 4.31 | 19.31 ± 10.47 | 21.91 ± 5.44 | 17.68 ± 7.35 | 33.57 ± 37.73 |
| Inclusive graphic skewness | 0.44 ± 0.04 | 0.51 ± 0.22 | 0.25 ± 0.04 | 0.66 ± 0.04 | 0.77 ± 0.04 | 0.32 ± 0.03 |
| Graphic kurtosis | 1.14 ± 0.06 | 0.91 ± 0.13 | 1.11 ± 0.04 | 1.50 ± 0.19 | 1.24 ± 0.26 | 1.10 ± 0.05 |
| Geometric STD of high region | 2.43 ± 0.15 | 3.62 ± 1.86 | 1.79 ± 0.08 | 3.61 ± 0.26 | 5.45 ± 0.62 | 1.98 ± 0.09 |
| Geometric STD of low region | 2.91 ± 0.25 | 4.69 ± 1.70 | 2.13 ± 0.10 | 3.07 ± 0.40 | 2.98 ± 0.63 | 2.32 ± 0.29 |
| Geometric STD of total region | 2.66 ± 0.16 | 3.77 ± 0.17 | 1.96 ± 0.08 | 3.32 ± 0.24 | 3.99 ± 0.25 | 2.14 ± 0.17 |
| Width | | | | | | |
| Statistical skewness | 2.23 ± 0.74 | 1.53 ± 0.36 | 2.15 ± 0.91 | 2.59 ± 0.41 | 2.14 ± 0.25 | 1.45 ± 0.48 |
| Statistical kurtosis | 11.63 ± 12.41 | 3.84 ± 2.09 | 15.50 ± 12.13 | 11.82 ± 4.34 | 7.67 ± 2.48 | 7.05 ± 4.75 |

Note: The data reported were: mean ± standard deviation of 10 image replications.

digital images and measured directly. Only possible loss of accuracy stems from low resolution, poor image quality, less contrast between object and background, improper thresholds, and faulty measurement algorithms. Comparing with the caliper dimensions of Basmati rice, the machine vision method had an accuracy in excess of 98.9% (mean absolute error = 1.11 ± 0.80%). Since least dimension measurable with machine vision at 6350 DPI is 0.004 mm and by digital calipers is 0.01, the error observed can be attributed to unrepeatability and error in manual measurements.

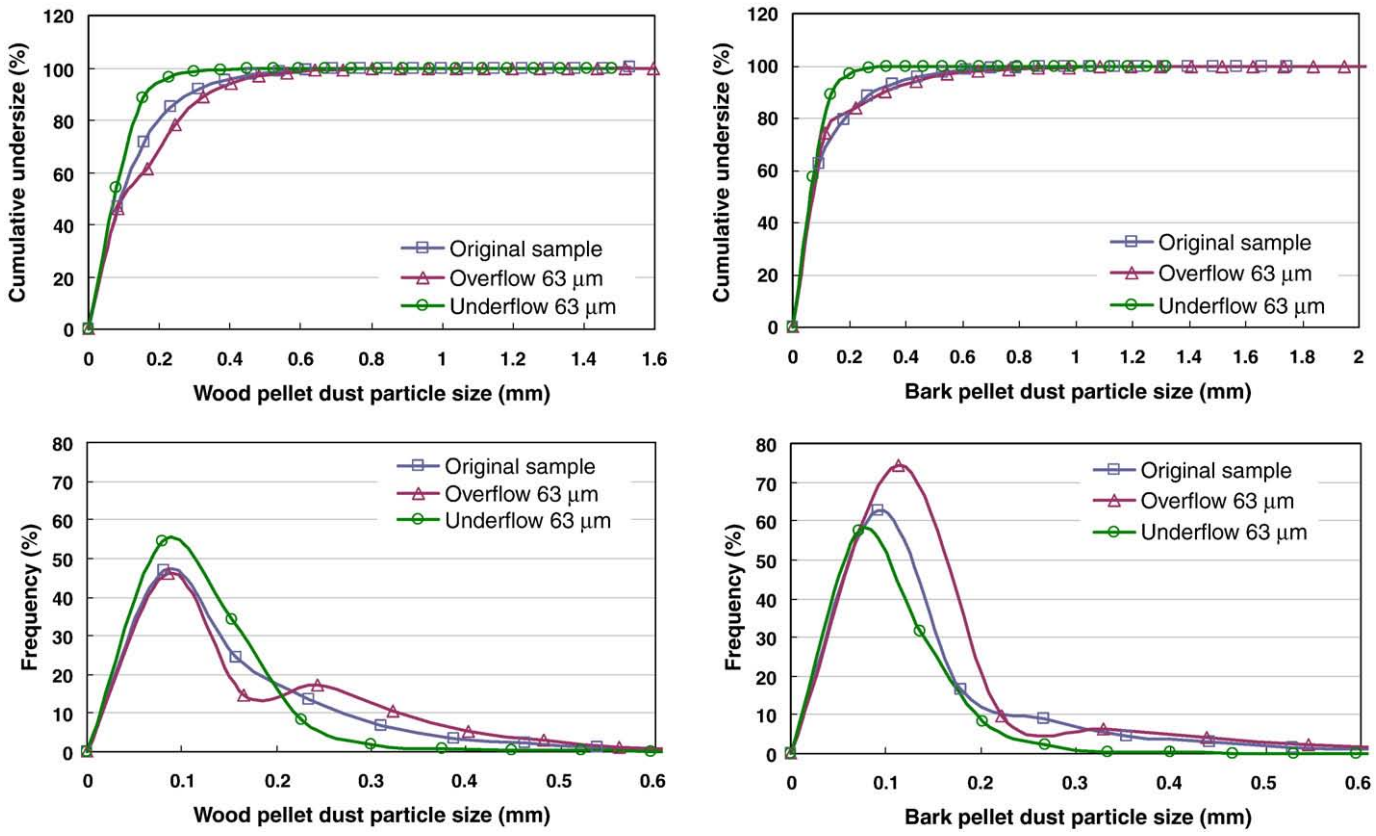


**Fig. 5.** Typical cumulative and frequency distribution of original and subsamples separated using 230 mesh sieve (63 μm).

### 3.6. Comparison between experimental mechanical sieving and machine vision analysis

Particle size distribution analysis from the two methods in the form of percentages of particles retained on sieves and cumulative particles retained showed comparable results (Fig. 6). In the absence of a standard reference method, it is not possible to decide which method is superior; however, Fig. 6 may serve to spot excessive departure (if present) between methods studied. The observed deviations can be attributed to the differing mechanisms of particle separation and grouping between the methods. Mechanical sieving is essentially a width-based separation, while the present machine vision is truly length-based separation. The mechanical sieving was already shown to be not eliminating the "falling-through" effect of longer particles through smaller size sieve openings [5]. In addition, clogging of sieve openings cannot be completely avoided owing to electrostatic forces of fine dust particles. Consistent less number of particles retained for both materials in the pan with mechanical sieving compared to machine vision method (Fig. 6) may be due to sieve clogging phenomenon. The reference materials as expected were retained on respective sieves (not shown in Fig. 6) as follows: 16% on 200 mesh, and 84% on 230 mesh for Pittsburgh steam coal; and 100% on 230 mesh for Lycopodium spores. These results as well demonstrate the effectiveness of mechanical sieving of uniform spherical particles. It should be noted that only 19 standard sieves are available in the airborne dust particle dimension range of $\leq$0.5 mm, while the sieveless machine vision method used more than 979 virtual sieves (Table 2) in the analysis. Since both the methods were quite comparable, the machine vision method can be advantageously utilized in place of the expensive and laborious mechanical sieving.

### 3.7. Limitations and merits of the machine vision plugin in airborne dust size determination

The limitations of the developed machine vision plugin in measurement of airborne dust particle dimensions are

1) The resolution of the imaging device limits the accuracy of measurement.
2) Unlike physical methods, such as mechanical sieving, the quantity of sample utilized is very small (a few milligrams), which forces the sample to be highly representative for reproducible results.
3) Layout of particles in singulated arrangement is a bit time consuming.
4) Non-singulated arrangement of particles will lead to overestimation of measured dimensions.
5) Deviation from appropriate threshold limits, especially with manual thresholding, will impair the accuracy.

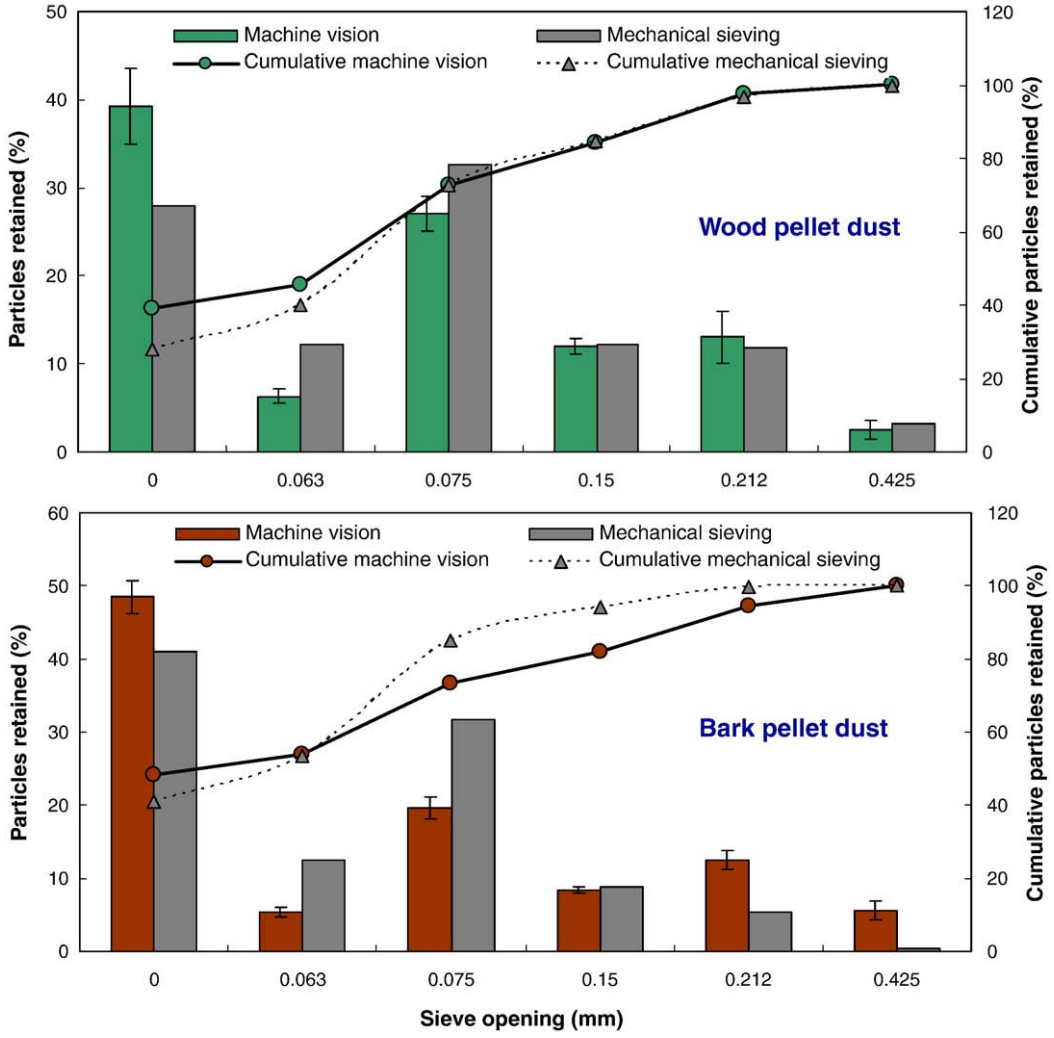


**Fig. 6.** Comparison between experimental mechanical sieving and machine vision particle size distribution analysis for original wood and bark pellet airborne dust samples.

6) A scanty possibility exists of improper width measurement only when the centroid of a curved particle falls over another encroaching particle.
7) High resolution images in combination with large physical dimension of image makes the image file size very large (in the order of GB) that cannot be handled by personal computers with 32 bit microprocessor.

Merits of developed plugin and machine vision method in relation to the present airborne dust particle size and size distribution determination and in general include

1) accuracy of measurement,
2) speedy calculations and automated analysis (Present work: mean of 587–1683 particles/s),
3) measurement of true length and width of particles through respective Feret's diameter and pixel-march techniques,
4) distinct particles grouped and particle size distribution analyzed in a sieveless manner,
5) the sieveless analysis producing ultimate grouping of particles is equivalent to involving an unlimited number of sieves based on the sample's number of distinct particles (Present work: 979–1401 mean distinct particles),
6) direct and nondestructive method of measurement,
7) desired parameters of size distribution and graphical outputs can be coded into the plugin,
8) algorithms are tailor-made to tackle different requirements (size and shape) of particles size and size distribution,
9) wide user accessibility by using ImageJ with Java compiler, and
10) cost-effectiveness achieved because of the utilization of an image processing freeware ImageJ, and the only expenditure required is the affordable commercial document flatbed scanner.

## 4. Conclusions

Size and size distribution determination of airborne dust particles from wood and bark pellets that can only be attained presently using sophisticated instruments can be also effectively accomplished using a user-coded machine vision ImageJ plugin to analyzed unsophisticated scanned images. The machine vision method with the developed plugin was accurate (>98.9%), quick (<8 s per image), reproducible, and highly inexpensive. Minute airborne dust particles of dimensions greater than 4 μm can be imaged utilizing flatbed scanner with resolution of 6350 DPI; however, still finer particles require proportionately increased DPI images but need specialized computing resources. Automatic threshold limits of ImageJ that leaves a "halo effect" around the particles grey-scale image gives the best result for binary image conversion. Wood pellet airborne dust particles are shorter than that of bark pellets. Arithmetic and geometric mean lengths of wood pellet airborne dust particles were $0.1138 \pm 0.0123$ and $0.0736 \pm 0.0076$ mm, while that of bark dust were $0.1181 \pm 0.0149$ and $0.0607 \pm 0.0071$ mm, respectively. The dust particles were elongated having length/width ratios in the range of 2.5 to 3.8. Clear division of subsamples based on length by standard 230 mesh (63 μm) cannot be achieved by sieving, owing to perpendicular "falling-through" effect of longer particles and electrostatic forces among the particles. Some of the overflow subsamples (>63 μm) exhibited "multimodality," while underflow subsamples (<63 μm) exhibited smooth variation of length. The airborne dust particles of wood and bark pellets were non-uniform, dominated by finer particles, "positively skewed" with very "finely skewed classification," "leptokurtic," and belonged to "very well sorted" category. Results of experimental mechanical sieving and machine vision analysis of airborne dust particles were found to be comparable. The machine vision method of analyzing size and size distribution of airborne dust and similar particles has a great potential to be considered as a standardized method of measurement and analysis.

## Acknowledgements

Financial support from the Natural Sciences and Engineering Research Council of Canada (NSERC: CRDPJ 342219-06, UBC PG11R82830) and Wood Pellets Association of Canada (WPA: UBC PG11R42500) is gratefully acknowledged.

## Appendix A. Descriptive parameters of particle size distribution

| Parameter | Formula |
|---|---|
| Average length (mm) | $\overline{L} = \sum_{i=1}^{N} L_i / N$ |
| Average width (mm) | $\overline{W} = \sum_{i=1}^{N} W_i / N$ |
| Standard deviation ($Y = L, W$) (mm) | $s = \sqrt{\sum_{i=1}^{N} (Y_i - \overline{Y})^2 / (N-1)}$ |
| ASABE geometric mean length (mm) | $X_{gl} = \ln^{-1}\left[\frac{\sum (N_i \times \ln X_i)}{\sum N_i}\right]$ |
| ASABE geometric mean length STD (mm) | $S_{gl} = \ln^{-1}\left[\frac{\sum \left(N_i (\ln X_i - \ln X_{gl})^2\right)}{\sum N_i}\right]^{\frac{1}{2}}$ |
| Graphic mean (mm) | $\overline{L}_g = \frac{D_{16} + D_{50} + D_{84}}{3}$ |
| Inclusive graphic STD | $\mathrm{STD}_{ig} = \left[\frac{D_{84} - D_{16}}{4}\right] + \left[\frac{D_{95} - D_5}{6.6}\right]$ |
| Uniformity index (%) | $I_u = \frac{D_5}{D_{90}} \times 100$ |
| Size grade number (mm) | $N_{sg} = D_{50} \times 100$ |
| Size range variation coefficient (%) | $S_v = \frac{D_{84} - D_{16}}{2D_{50}} \times 100$ |
| Relative span | $S_l = \frac{D_{90} - D_{10}}{D_{50}}$ |
| Coefficient of uniformity | $C_u = \frac{D_{60}}{D_{10}}$ |
| Coefficient of gradation | $C_g = \frac{D_{30}^2}{D_{10} \times D_{60}}$ |
| Statistical length skewness | $L_s = \frac{\sum_{i=1}^{N} (L_i - \overline{L})^3}{(N-1)s^3}$ |
| Statistical width skewness | $W_s = \frac{\sum_{i=1}^{N} (W_i - \overline{W})^3}{(N-1)s^3}$ |
| Statistical length kurtosis | $L_k = \frac{\sum_{i=1}^{N} (L_i - \overline{L})^4}{(N-1)s^4} - 3$ |
| Statistical width kurtosis | $W_k = \frac{\sum_{i=1}^{N} (W_i - \overline{W})^4}{(N-1)s^4} - 3$ |
| Inclusive graphic skewness | $S_{ig} = \left[\frac{D_{84} + D_{16} - 2D_{50}}{2(D_{84} - D_{16})}\right] + \left[\frac{D_{95} + D_5 - 2D_{50}}{2(D_{95} - D_5)}\right]$ |
| Graphic kurtosis | $K_g = \left[\frac{D_{95} - D_5}{2.44(D_{75} - D_{25})}\right]$ |
| Geometric STD of high region | $\mathrm{STD}_h = \frac{D_{84}}{D_{50}}$ |
| Geometric STD of low region | $\mathrm{STD}_l = \frac{D_{50}}{D_{16}}$ |
| Geometric STD of total region | $\mathrm{STD}_t = \sqrt{\frac{D_{84}}{D_{16}}}$ |

## References

[1] V. Mody, R. Jakhete, Dust control handbook for minerals processing, A mining research contract report, Contract No. J0235005, February 1987, Bureau of Mines U.S. Department of the Interior, 1987.
[2] Wood Pellets Association of Canada, http://www.pellet.org/Site/Forms/ViewPage.aspx?PageID=318, (Accessed July 2009).
[3] A.R. Womac, C. Igathinathane, P. Bitra, P. Miu, T. Yang, S. Sokhansanj, S. Narayan, Biomass pre-processing size reduction with instrumented mills, ASABE Paper No. 076046, ASABE, St. Joseph, MI, 2007.
[4] C. Igathinathane, L.O. Pordesimo, W.D. Batchelor, Ground biomass sieve analysis simulation by image processing and experimental verification of particle size distribution, ASABE Paper No. 084126, ASABE, St. Joseph, MI, 2008.
[5] C. Igathinathane, L.O. Pordesimo, E.P. Columbus, W.D. Batchelor, S. Sokhansanj, Sieveless particle size distribution analysis of particulate materials through computer vision, Computers and Electronics in Agriculture 66 (2009) 147–158.
[6] D.C. Slaughter, D.K. Giles, D. Downey, Autonomous robotic weed control systems: a review, Computers and Electronics in Agriculture 61 (2008) 63–78.
[7] C.J. Du, D.W. Sun, Recent developments in the applications of image processing techniques for food quality evaluation, Trends in Food Science & Technology 15 (2004) 230–249 231.
[8] T. Brosnan, D.W. Sun, Inspection and grading of agricultural and food products by computer vision systems — a review, Computers and Electronics in Agriculture 36 (2002) 193–213.
[9] K.D. Friedland, D. Ama-Abasi, M. Manning, L. Clarke, G. Kligys, R.C. Chambers, Automated egg counting and sizing from scanned images: rapid sample processing and large data volumes for fecundity estimates, Journal of Sea Research 54 (2005) 307–316.

[10] W.S. Rasband, ImageJ. U.S. National Institutes of Health, Bethesda, MD, USA, 2007 http://rsb.info.nih.gov/ij/index.html (Accessed July 2009).
[11] W. Bailer, Writing ImageJ Plugins — A Tutorial. Version 1.71, 2006 http://rsb.info.nih.gov/ij/download/docs/tutorial171.pdf (Accessed July 2009).
[12] W. Burger, M.J. Burge, Digital Image Processing — An Algorithmic Introduction using Java, Springer, New York, N.Y., 2008.
[13] C. Igathinathane, L.O. Pordesimo, E.P. Columbus, W.D. Batchelor, S.R. Methuku, Shape identification and particles size distribution from basic shape parameters using ImageJ, Computers and Electronics in Agriculture 63 (2008) 168–182.
[14] C. Igathinathane, L.O. Pordesimo, W.D. Batchelor, Major orthogonal dimensions measurement of food grains by machine vision using ImageJ, Food Research International 42 (2009) 76–84.
[15] M.A. Shahin, S.J. Symons, Seed sizing from images of non-singulated grain samples, Canadian Biosystems Engineering 47 (2005) 49–54.
[16] R.L. Folk, W.C. Ward, Brazos River bar: a study in the significance of grain size parameters, Journal of Sedimentary Petrology 27 (1957) 3–26.
[17] S.J. Blott, K. Pye, GRADISTAT: a grain size distribution and statistics package for the analysis of unconsolidated sediments, Earth Surface Processes and Landforms 26 (2001) 1237–1248.